ACS APPLIED MATERIALS & INTERFACES

Research Article

www.acsami.org

Graphene Oxide–Silver Nanocomposite As a Highly Effective Antibacterial Agent with Species-Specific Mechanisms

Jia Tang, Qian Chen, Ligeng Xu, Shuai Zhang, Liangzhu Feng, Liang Cheng, Huan Xu, Zhuang Liu,* and Rui Peng*

Institute of Functional aNano & Soft Materials (FUNSOM), Jiangsu Key Laboratory for Carbon-Based Functional Materials & Devices, Soochow University, Suzhou, Jiangsu 215123, China

Supporting Information

ABSTRACT: Recently, graphene oxide (GO) based nanocomposites have raised significant interests in many different areas, one of which being antibacterial agents where sliver nanoparticle (AgNPs) anchored GO (GO–Ag) has shown promising potential. However, to our best knowledge, factors affecting its antibacterial activity as well as the underlying mechanism remain unclear. In this study, we fabricate GO–Ag nanocomposites with different AgNPs to GO ratios and carefully investigate their antibacterial activities against both the Gram-negative (G−) bacteria *Escherichia coli* (*E. coli*) and the Gram-positive (G+) bacteria *Staphylococcus aureus* (*S. aureus*). We discover that, compared to AgNPs, GO–Ag nanocomposite with an optimal ratio of AgNPs to GO is much more effective and shows synergistically enhanced, strong antibacterial activities at rather low dose (2.5 μg/mL). The GO–Ag nanocomposite is more toxic to *E. coli* than that to *S. aureus*. The antibacterial effects of GO–Ag nanocomposite are further investigated, revealing distinct, species-specific mechanisms. The results demonstrate that GO–Ag nanocomposite functions as a bactericide against the G− *E. coli* through disrupting bacterial cell wall integrity, whereas it exhibits bacteriostatic effect on the G+ *S. aureus* by dramatically inhibiting cell division. Our work not only highlights the great promise of using GO–Ag as a highly effective antibacterial agent but also provides more in-depth understandings of the interactions between microorganisms and GO-based nanocomposites.

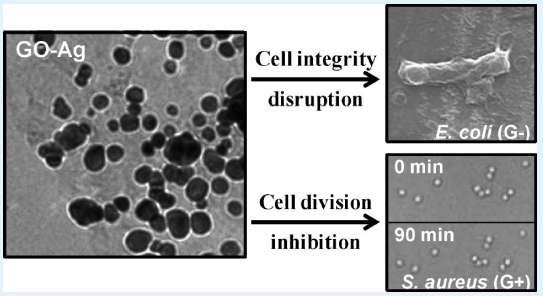

KEYWORDS: *sliver nanoparticle anchored graphene oxide (GO–Ag), antibacterial, species-specific mechanism, bactericide, bacteriostatic agent, graphene oxide*

1. INTRODUCTION

Antibacterial materials and agents play important roles in treating infectious diseases caused by pathogenic bacteria. However, the wide use of antibiotics leads to the rise of microbial drug resistance, resulting in poor treatment efficacy and significant economic losses.[1−4] The rapid development of nanotechnology in the past decades opens up new opportunities in antibacterial research.[5−7] Among many nanomaterials reported as antibacterial agents, silver nanoparticles (AgNPs) with excellent antibacterial activity have been the most widely explored and are currently being used in a number of commercial products.[8−12]

Graphene since its discovery has received great attention in many different areas.[13−26] In the field of biomedicine, functionalized graphenes have been used for drug delivery,[27−35] gene transfection,[27,36−38] biosensing,[13,15,39−42] as well as tumor imaging and photothermal therapy.[19,20,38,43−46] Recently, the potential antibacterial applications of graphene and graphene-based nanocomposites have also attracted considerable interests,[47−51] although whether and how graphene oxide (GO) presents antibacterial activity are still under debate.[48,50,52] By growing AgNPs on the surface of GO, several groups via different approaches have synthesized GO–Ag nanocomposites with significant antibacterial activities.[53−64] However, despite these independent demonstrations of the strong antibacterial ability of GO–Ag, to our best knowledge, it is still not fully clear whether there is any advantages of using GO–Ag as a new generation of antibacterial agent with unique, or synergistic efficacy, compared to the simple combination of separated GO and AgNPs and what the antibacterial mechanisms of GO–Ag toward different types of bacteria are.

To address these questions, in this work, GO–Ag nanocomposites with different AgNPs to GO ratios are synthesized using a simple one-pot boiling reaction. The antibacterial activities of GO–Ag nanocomposites are investigated using Gram-negative (G−) bacteria *Escherichia coli* (*E. coli*) and Gram-positive (G+) bacteria *Staphylococcus aureus* (*S. aureus*) as two model microorganisms.[65] The effects of different ratios of AgNPs to GO and dosages on the antibacterial activity of this nanocomposite are also systematically investigated. Our results reveal that, compared with AgNPs or the simple mixture of GO and AgNPs, GO–Ag nanocomposite with the optimal

Received: February 9, 2013
Accepted: April 15, 2013
Published: April 15, 2013

   dx.doi.org/10.1021/am4005495 | ACS Appl. Mater. Interfaces 2013, 5, 3867−3874

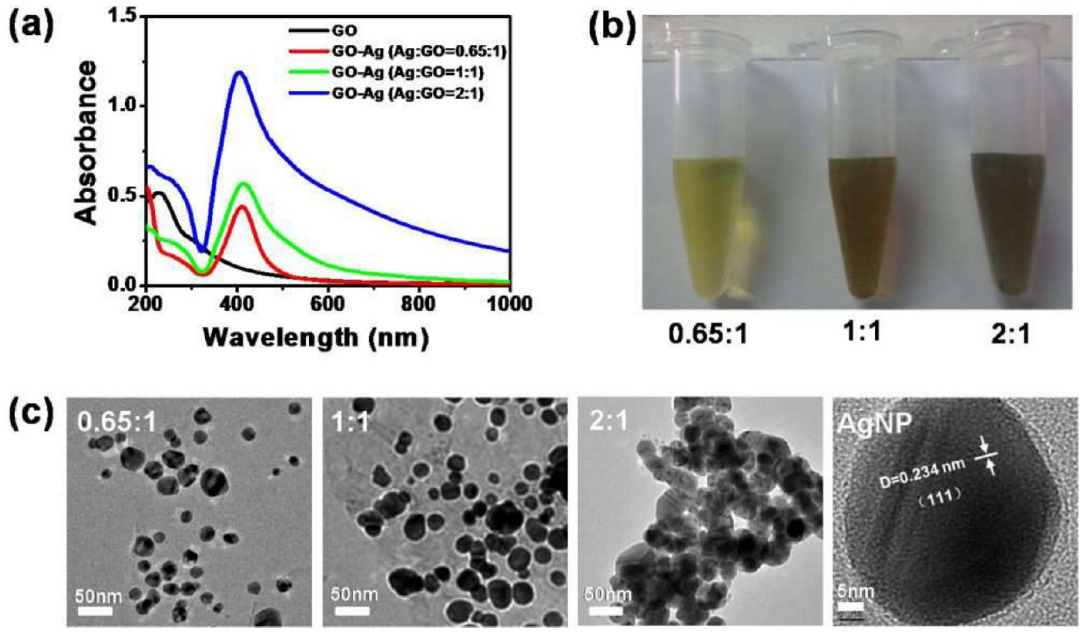

Figure 1. Characterization of the three types of GO−Ag nanocomposites with different AgNPs to GO ratios. (a) UV−vis absorption spectra of GO and GO−Ag nanocomposites. (b) Photos showing three types of GO−Ag nanocomposites dispersed in water. (c) TEM images of three types of GO−Ag nanocomposites. The right one is a HRTEM image of an AgNP grown on the GO sheet.

AgNPs to GO ratio shows remarkably increased antibacterial activity even at very low concentrations (2.5 μg/mL), likely owing to its unique physicochemical property. To investigate the underlying antibacterial mechanisms of GO−Ag nanocomposite, morphology changes and division of bacterial cells are studied. Interestingly, we uncover that the GO−Ag nanocomposite exhibits higher toxicity against *E. coli* than *S. aureus*, and it functions on these bacteria through distinct, species-specific mechanisms. Upon treatment with GO−Ag nanocomposite, the G− *E. coli* shows disrupted bacterial cell wall/membrane, while the G+ *S. aureus* shows little bacterial cell wall integrity damaging but significantly inhibited cell division. Our study offers in-depth understandings of the antibacterial behaviors of the GO−Ag nanocomposite, further highlighting its promising potential as a highly effective antibacterial agent with low toxicity to mammalian cells.

2. EXPERIMENTAL SECTION

2.1. Synthesis and Characterization of GO−Ag Nanocomposites. GO was synthesized by the modified Hummers' method from flake graphite according to our previously reported protocol.[35,66] GO−Ag nanocomposite was prepared by reducing $AgNO_3$ by sodium citrate in the presence of GO suspension. In brief, 1.3 mL of GO suspension (1.35 mg/mL) was added into 98.7 mL of deionized water. The desired amount (18, 36, or 54 mg) of $AgNO_3$ powder was then added to the GO solution. After the reaction solution was boiled, the desired amount (20, 40, or 60 mg) of sodium citrate powder was quickly added to the reaction mixture which was then further boiled for 1 h. In this reaction process, it is likely that the reduction of Ag first occurs on the defects of the GO sheets, forming small Ag nucleation centers, from which AgNPs are grown. The synthesized GO−Ag nanocomposites were purified via filtration and repeated washing for three times using deionized water and, then, redispersed in deionized water.

The concentration of GO was calculated using the absorbance at 230 nm (mass extinction coefficient of 65 mg mL^{-1} cm^{-1}).[67] The amount of Ag in GO−Ag nanocomposites was measured by complexometric titration.[68] All GO−Ag nanocomposites were characterized by transmission electron microscopy (TEM; Tecnai G20 F20, FEI), X-ray diffraction (XRD; Empyrean, PANalytical), and energy-dispersive X-ray spectroscopy (EDS; Tecnai G20 F20, FEI).

2.2. Bacterial Culture. *E. coli* and *S. aureus* were cultured in Lysogeny broth (LB) medium and incubated in a shaking incubator at 37 °C overnight. The next day, before treatments, the bacterial cells were brought into log phase by reinoculating the overnight culture 1:100 into fresh media and growing at 37 °C in the shaking incubator for 2−3 h till an optical density at 600 nm (OD_{600}) of 0.5 was reached.

2.3. Antibacterial Activity Tests. Log phase bacteria cells were inoculated 1:10 in fresh LB medium containing different nanomaterials or water as indicated in the text, and then incubated for 2.5 h at 37 °C in the shaking incubator. The metabolic activities of bacterial cells in these cultures were analyzed using the colorimetric 3-(4,5-dimethylthiazol-2-yl)-2,5-diphenyl tetrazolium bromide (MTT) assay. The cultures were diluted and dispensed in 96-well plates (100 μL per well). For each culture, a well with LB medium containing the same amount of nanomaterials but no bacterial cells was set as the blank, and all measurements were carried out in triplicate or quadruplicate. The MTT assay was carried out as described.[69]

The numbers of viable bacterial cells in the above cultures were analyzed using the colony forming units (CFU) counting. Briefly, gradient dilutions of each culture were plated in triplicate on LB-agar plates, incubated at 37 °C for 14 h, and the bacterial colonies formed were counted and recorded.

Minimum inhibitory concentration (MIC) of GO−Ag nanocomposite (Ag:GO = 1:1) was also determined by standardized agar dilution.[70] Briefly, Log phase *E. coli* and *S. aureus* cells (10^4 CFU) were spotted on a series of agar plates containing dilutions of the GO−Ag and incubated overnight at 37 °C. The MIC value is defined as the lowest concentration of GO−Ag at which no visible bacterial growth is observed. For comparison, the MIC of ampicillin and kanamycin against each strain was also determined following the same protocol.

2.4. Fluorescent-Based Cell Wall/Membrane Integrity Assay. Log phase *E. coli* and *S. aureus* cells were inoculated 1:10 in fresh LB broth with or without 10 μg/mL GO−Ag nanocomposite (Ag:GO = 1:1), respectively. After growth for 2.5 h at 37 °C in the shaking incubator, the bacteria were collected by centrifugation, stained with propidium iodide (PI, 1 μg/mL) for 15 min, counterstained with 4′-6-diamidino-2-phenylindole (DAPI, 5 μg/mL) for 5 min in the dark, and then imaged using a Leica TCS SP5 II confocal microscope.

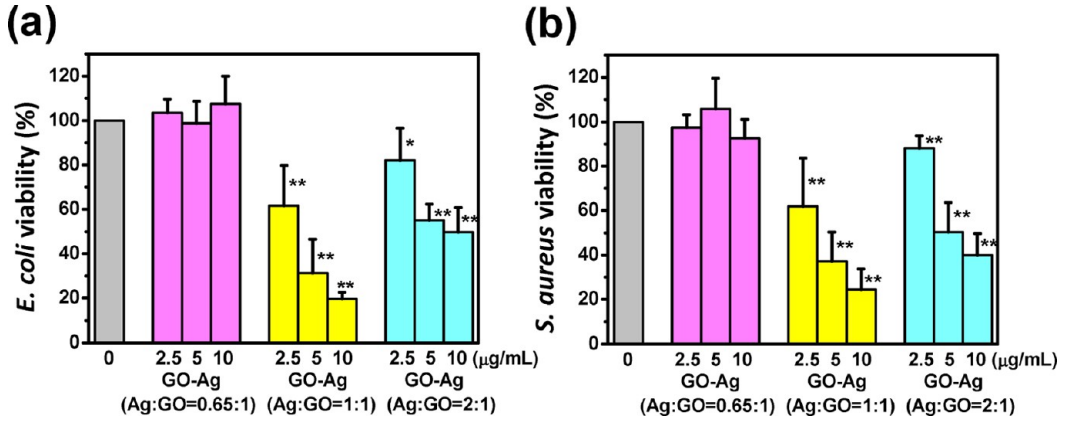

Figure 2. Bacterial cell viability of *E. coli* (a) and *S. aureus* (b) after treatments of the three types of GO−Ag nanocomposites at indicated final concentrations. Error bars represent the standard deviations ($n \geq 4$). *$P < 0.05$, **$P < 0.01$.

2.5. Morphological Characterization of Bacteria. Bacterial cells were collected and washed twice with PBS, followed by fixing with 2.5% glutaraldehyde solution for 2 h. The samples were dehydrated with sequential treatment of 50, 70, 85, 90, and 100% ethanol for 10 min, gold sputter-coated, and imaged using a scanning electron microscope (SEM; Quanta 200FEG, FEI).

2.6. Time-Lapse Photography of Bacterial Growth. Time-lapse photography of bacterial growth and division was carried out following a previous protocol[71] with modifications. A 70 μL LB medium containing 3% (w/v) agar with (GO−Ag^+) or without (GO−Ag^-) 10 μg/mL GO−Ag nanocomposite (Ag:GO = 1:1) was plated between two clean round coverslips to form a 1 mm-thick LB-agar pad with a flat, smooth surface. Individual GO−Ag nanocomposite (Ag:GO = 1:1) treated *S. aureus* cells were sandwiched between a glass bottom cell culture dish and the GO−Ag^+ LB-agar pad. Untreated *S. aureus* cells and the GO−Ag^- pad were sandwiched as control. The bacteria growth was monitored and imaged using the confocal microscope while incubating at 37 °C in the temperature-control accessory.

2.7. Bacterial Genomic DNA Analysis. A 1 mL portion of bacterial suspension culture was harvested by centrifugation. The bacterial genomic DNA was extracted using the cetyl trimethyl ammonium bromide (CTAB)/NaCl method as described,[72] separated on 0.8% agarose gel electrophoresis, and visualized by ethidium bromide (EB) staining.

2.8. Cell Viability Assay of Mammalian Cells. HeLa cells and HEK 293T cells were cultured in Dulbecco's modified Eagle's medium (DMEM) supplemented with 10% fetal bovine serum (FBS) at 37 °C. Both cells were treated with various concentrations of GO−Ag nanocomposite (Ag:GO = 1:1) at 37 °C for 24 h, and the cell viabilities were analyzed using MTT assay as described.[73]

3. RESULTS AND DISCUSSION

3.1. Synthesis and Characterization of GO−Ag Nanocomposites. An environmentally friendly and facile method was developed for the preparation of GO−Ag nanocomposite using sodium citrate as the reducing agent. To systematically investigate the antibacterial activity of GO−Ag nanocomposite, three types of GO−Ag nanocomposites with different AgNPs to GO ratios (measured by complexometric titration to be 0.65, 1, and 2) were synthesized. As shown in Figure 1a, compared with the characteristic absorption peak of GO at 230 nm, these nanocomposites displayed an absorption peak at about 410 nm with different peak values, suggesting that different amounts of AgNPs were successfully deposited on the GO sheets. With GO sheets as the supporting material, which would effectively stabilize AgNPs, keeping them from aggregation, all three nanocomposites exhibited excellent water-dispersibility (Figure 1b), which is of great importance for their bioapplications. TEM images showed that AgNPs deposited on the GO sheets were spherical with an average diameter of about 46 nm for GO−Ag (Ag:GO = 0.65:1) and GO−Ag (Ag:GO = 1:1) and about 68 nm for GO−Ag (Ag:GO = 2:1) (Figure 1c and Supporting Information, Figure S1), and their crystal structures were further confirmed using high-resolution TEM (HRTEM; Figure 1c) and XRD (Supporting Information, Figure S2a). The chemical composition of GO−Ag nanocomposite was also analyzed by the EDS spectrum showing no contamination peak (Supporting Information, Figure S2b).

3.2. Optimized, Highly Effective Antibacterial Activity of GO−Ag Nanocomposite. The antibacterial activities of these three types of GO−Ag nanocomposites against G− and G+ bacteria were investigated using *E. coli* and *S. aureus* as model organisms, respectively. Log phase bacterial cells actively dividing were used in all experiments. As shown in Figure 2, at concentrations lower than 10 μg/mL, all nanocomposites except GO−Ag (Ag:GO = 0.65:1) significantly decreased viabilities of both *E. coli* and *S. aureus* cells in a dose-dependent manner. Among these three nanocomposites, GO−Ag (Ag:GO = 1:1) showed the strongest antibacterial effect in that at a concentration as low as 2.5 μg/mL, it reduced the viabilities of both *E. coli* and *S. aureus* cells by 40%, and at a concentration of 10 μg/mL, it decreased the viabilities of *E. coli* and *S. aureus* cells to 20% and 24%, respectively. The GO−Ag (Ag:GO = 0.65:1) did show obvious antibacterial effect but required much higher concentrations (≥25 μg/mL), indicating the weakest antibacterial activity among the three (Supporting Information, Figure S3). The data suggest that the ratio of AgNPs/GO is very important for the antibacterial activity of GO−Ag nanocomposite. Therefore, the GO−Ag with the ratio of Ag:GO = 1:1, which shows the highest antibacterial activity among the three, was chosen in the following experiments.

3.3. Synergistically Enhanced Antibacterial Activity upon AgNPs Anchoring on GO Sheets. In the above results, despite the finding that the ratio of AgNPs/GO plays an important role in the antibacterial activity of GO−Ag nanocomposites, all three of them exhibited increased antibacterial activities when compared to pure AgNPs, which could only decrease the viabilities of *E. coli* and *S. aureus* cells to about 45% even at a concentration as high as 100 μg/mL (Supporting Information, Figure S4). We then wondered whether the significant antibacterial effect of GO−Ag nanocomposite could be due to a synergistic effect of GO and

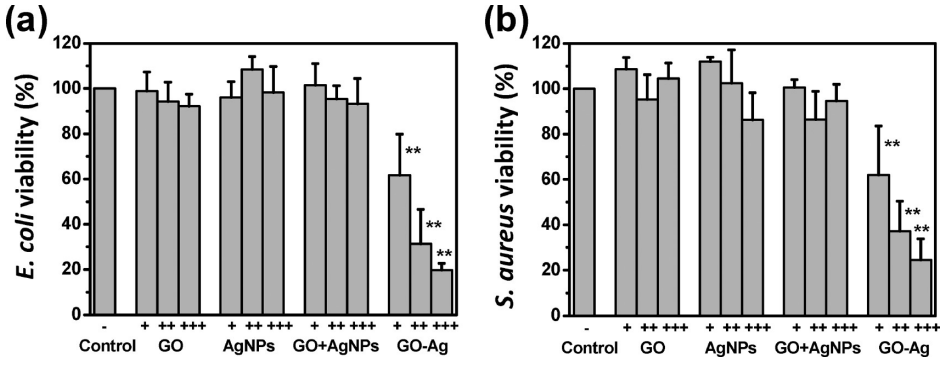

Figure 3. Bacterial cell viability of *E. coli* (a) and *S. aureus* (b) after treatments with either pure GO sheets (GO), pure AgNPs (AgNPs), GO−Ag nanocomposite (Ag:GO = 1:1) (GO−Ag), or the mixture of GO and AgNPs (GO + AgNPs) at different final concentrations. +, ++, and +++ represent equivalent GO or Ag concentrations at 1.25, 2.5, and 5 μg/mL, respectively, for all different samples. Error bars represent the standard deviations ($n \geq 3$). $^{**}P < 0.01$.

AgNPs or just an additive effect of the two types of nanomaterials. To address this question, bacteria cells were treated with pure GO, pure AgNPs, GO−Ag nanocomposite (Ag:GO = 1:1), and the mixture of GO and AgNPs, respectively. As shown in Figure 3, unlike the GO−Ag nanocomposite, pure GO, pure AgNPs, and their simple mixture at the same concentration as the working concentration of the nanocomposite showed no obvious effect on the viabilities of both *E. coli* and *S. aureus* cells. Therefore, the remarkably enhanced antibacterial activity of GO−Ag is not simply the additive effects of the two components, GO and AgNPs, separately functioning in this system but rather due to the unique physicochemical structure of this nanocomposite, which might provide a unique nanointerface for interacting with different microbes and would also facilitate the contact/interaction between AgNPs and GO sheets, inducing the synergistic effect. This might explain the necessity of the optimal AgNPs to GO ratio. As shown in the TEM data (Figure 1c and Supporting Information Figure S1), a ratio lower than 1:1 represents insufficient AgNPs on GO sheets, whereas a ratio higher than 1:1 (e.g., 2:1) not only results in larger AgNPs but also leads to partial aggregation of AgNPs on GO sheets, which in turn could alter the interface and reduce the active area for the interaction of AgNPs with GO sheets and/or the interaction of GO−Ag with microbes.

3.4. GO−Ag Nanocomposite Exhibited a Significantly Higher Antibacterial Activity against *E. coli* than *S. aureus*. The number of viable bacterial cells after GO−Ag treatment was further studied by CFU counting method. In the case of *S. aureus*, after treatment with 10 μg/mL GO−Ag nanocomposite for 2.5 h, 26% bacteria cells remained viable in the culture (Figure 4a), consistent with the results from the MTT assay (24%, Figure 2b). Surprisingly, as shown in Figure 4b, after the same treatment, nearly no *E. coli* bacterial colony on the LB-agar plate was formed and only 6% of *E. coli* cells remained viable in the treated culture, which was significantly lower than that of *S. aureus* (Figure 4a) and also lower than the 20% remaining viability measured using the MTT assay (Figure 2a). Since the result of an MTT assay can be affected by not only the total number of cells but also the succinate dehydrogenase activity of each cell, it is possible that some succinate dehydrogenase (or other reductase) activity remained detectable in nonviable *E. coli* cells, resulting in the higher cell viability measured using the MTT assay. Nevertheless, the CFU method directly measures the amount of viable cells while the

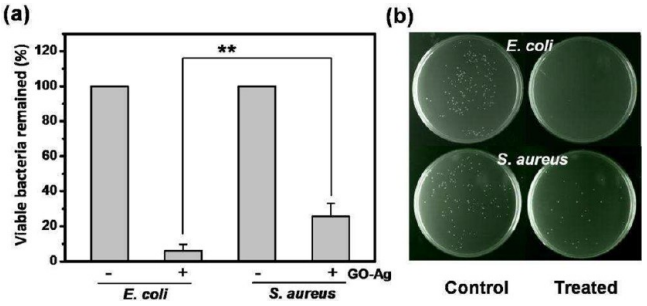

Figure 4. Viable bacteria remaining in the cultures of *E. coli* and *S. aureus* after being treated with 10 μg/mL GO−Ag nanocomposite (Ag:GO = 1:1) at 37 °C for 2.5 h. Representing photographs of bacterial colonies formed on LB-agar plates are shown in part b. Error bars represent the standard deviations ($n \geq 3$). $^{**}P < 0.01$.

MTT assay only measures residual enzyme activity; hence, the GO−Ag nanocomposite possesses a much higher antibacterial activity against the G− *E. coli* than the G+ *S. aureus*.

The susceptibilities of *E. coli* and *S. aureus* to the GO−Ag nanocomposite were also demonstrated by the MIC value, an important parameter to evaluate the bacterial susceptibility to a certain antibacterial agent; i.e., the lower the MIC, the higher the bacterial susceptibility, and, hence, the stronger the antibacterial activity. As shown in Table 1, no visible *E. coli*

Table 1. MIC Values of GO−Ag Nanocomposite (Ag:GO = 1:1) and Two Antibiotics against *E. coli* and *S. aureus*[a]

bacteria	GO−Ag (Ag:GO = 1:1) MIC (μg/mL)	kanamycin MIC (μg/mL)	ampicillin MIC (μg/mL)
E. coli	4	6	25
S. aureus	14	6	≤1

[a]The results were repeated at least 4 times.

growth can be observed on agar plates containing as low as 4 μg/mL of GO−Ag (Ag:GO = 1:1), while 14 μg/mL of GO−Ag (Ag:GO = 1:1) is required to fully inhibit the growth of *S. aureus*, indicating that *E. coli* is more susceptible to GO−Ag than *S. aureus*. Interestingly, when compared to the MICs of two commonly used antibiotics, ampicillin and kanamycin, the MIC of GO−Ag against *S. aureus* is higher than those of the two antibiotics, whereas in the case of *E. coli*, the MIC of GO−Ag drops to the lowest among the three, e.g. for the *E. coli* strain, which is just intermediately susceptible to ampicillin (a

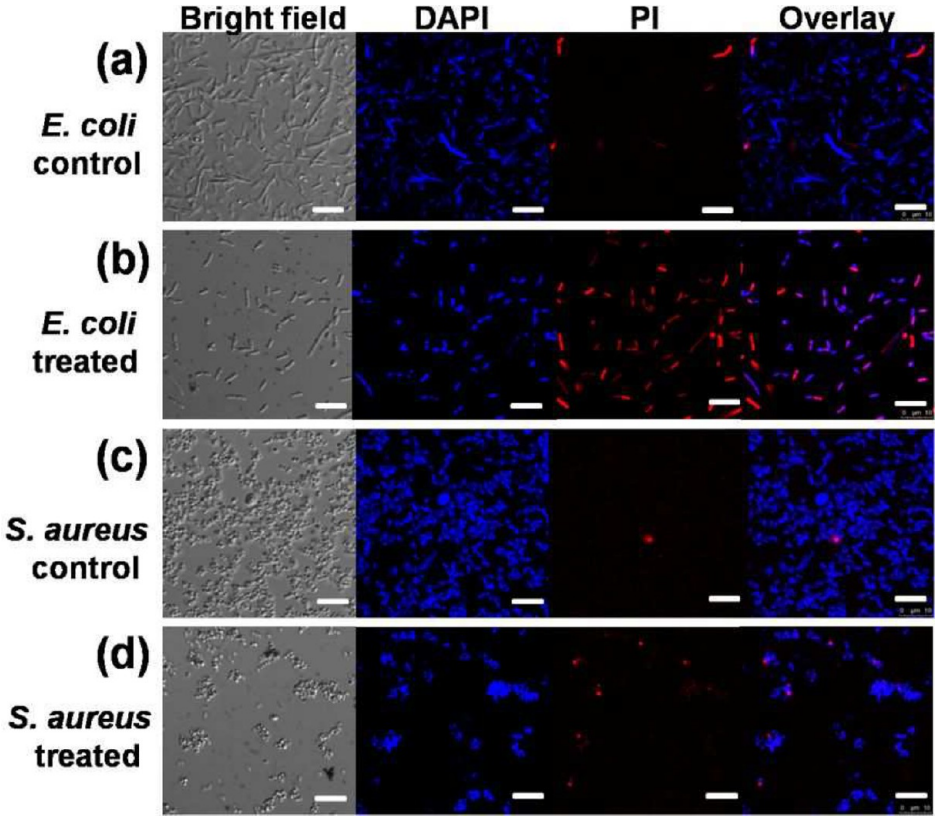

Figure 5. Confocal fluorescent images of live and dead bacterial cells after incubation with 10 μg/mL of GO−Ag nanocomposite (Ag:GO = 1:1) for 2.5 h: (a) *E. coli* no treatment; (b) *E. coli* with nanocomposites; (c) *S. aureus* no treatment; (d) *S. aureus* with nanocomposites. Blue fluorescence shows bacterial quasi nuclear stained with DAPI, while red fluorescence shows dead bacteria stained with PI. The scale bar is 10 μm.

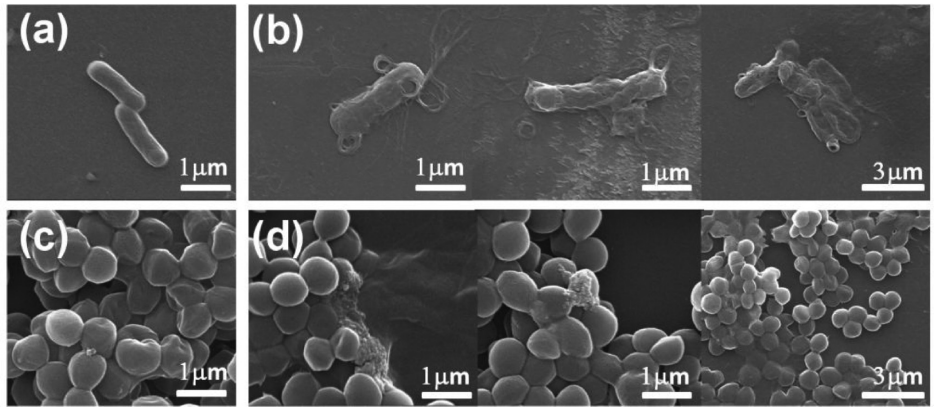

Figure 6. SEM images of *E. coli* cells (a and b) and *S. aureus* cells (c and d) without (a and c) and with (b and d) GO−Ag treatment at 10 μg/mL for 2.5 h.

relatively high MIC of 25 μg/mL), GO−Ag can be much more effective with an MIC of 4 μg/mL. These interesting variations of MICs between different bacteria species and antibacterial materials could suggest their distinct antibacterial mechanisms.

3.5. Cell Integrity Disruption of *E. coli* Induced by GO−Ag Nanocomposite. To further investigate the antibacterial mechanism of GO−Ag, two fluorescent nucleic acid dyes, DAPI and PI, were employed to stain the DNA of bacteria. DAPI labels both live and dead cells while PI can only penetrate cells with compromised or damaged membranes.[74] As shown in Figure 5a and c, there were few dead cells in untreated bacteria. In the treatment group of *E. coli*, almost all the bacteria were stained by PI (Figure 5b), indicating damaged cell walls and cell membranes and/or mass cell death upon GO−Ag exposure. In stark contrast, only very few *S. aureus* could be stained by PI in the treatment group (Figure 5d), suggesting that GO−Ag nanocomposite can selectively induce cell death of the G− *E. coli* but not the G+ *S. aureus* by disrupting cell wall/membrane integrity.

The results above were also cooperated by the morphological studies of bacteria using SEM. As shown in Figure 6a and c, untreated *E. coli* and *S. aureus* were typically rod-shaped and round-shaped, respectively, both with smooth and intact cell walls. After being treated with GO−Ag nanocomposite, the quantity of *E. coli* greatly decreased and cell walls became wrinkled and damaged, similar to previous reports.[48,52] The

shape and size of cells also changed dramatically, and for most of the *E. coli* cells, leakage of intracellular contents could be observed (Figure 6b). As for *S. aureus*, the morphologies of most of the survived cells remained unchanged with round-shape and smooth surface, while the leaking of intracellular contents could only be observed in very few cells (Figure 6d). It is likely that GO−Ag exhibited different impacts on the cell walls and cell membranes of G− and G+ bacteria, possibly due to the different structures and chemical compositions of their cell walls:[65] unlike G− bacteria, whose cell walls contain only one thin layer of peptidoglycan, G+ bacteria have multilayers of peptidoglycan in the cell wall, which might provide a better protection against GO−Ag.

3.6. Cell Growth Arrest of *S. aureus* Induced by GO−Ag Nanocomposite. The above results suggested that GO−Ag nanocomposite kills the G− *E. coli* through destroying bacterial cell membrane/wall integrity. Since the antibacterial effect of GO−Ag against *S. aureus* (G+) is also prominent, we further investigated the inhibitory mechanism of GO−Ag on *S. aureus*. We first examined whether the GO−Ag nanocomposite could induce damage to the bacterial genomic DNA, which, however, appeared to be unaffected for both *E. coli* and *S. aureus* cells after the treatment (Supporting Information, Figure S5). Next, we examined cell division of *S. aureus* by following cells' growth on a microscope stage in real time. Results showed that some of the untreated *S. aureus* cells began to divide within 30 min and most of them doubled within 60 min (Figure 7a).

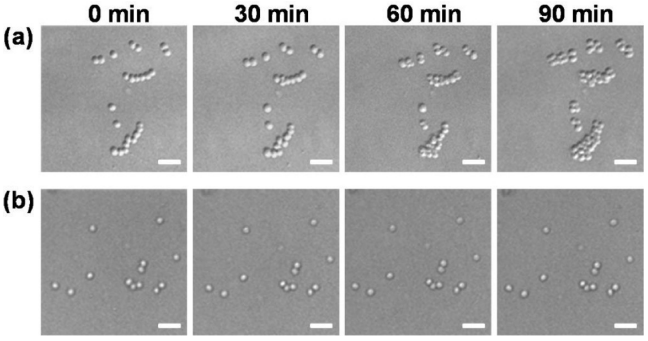

Figure 7. Real-time bacterial growth of *S. aureus*. (a) Normal cells plated on LB-agar pad. (b) Cells treated with 10 μg/mL GO−Ag nanocomposite (Ag:GO = 1:1) for 2.5 h before plated on LB-agar pad containing 10 μg/mL GO−Ag (Ag:GO = 1:1). The bacterial growth was monitored and imaged at indicated time intervals. The scale bar is 5 μm.

In contrast, on the GO−Ag containing LB-agar pad, no *S. aureus* cell divided within 90 min (Figure 7b), demonstrating severe inhibition of cell division of *S. aureus* by the GO−Ag nanocomposite.

3.7. Low Cytotoxicity of GO−Ag Nanocomposite toward Mammalian Cells. The cytotoxicity of the nanocomposite to mammalian cells was also investigated. As shown in Figure 8, after treated with GO−Ag nanocomposite (Ag:GO = 1:1) for 24 h at 10 μg/mL, the dose at which 94% *E. coli* cells were killed within 2.5 h, more than 80% of both HeLa cells and HEK 293T cells remained viable. Even at very high concentrations (up to 50 μg/mL), the viabilities of both cells remained above 65%, suggesting that GO−Ag nanocomposite may be a promising antibacterial agent with low toxicity to mammalian cells.

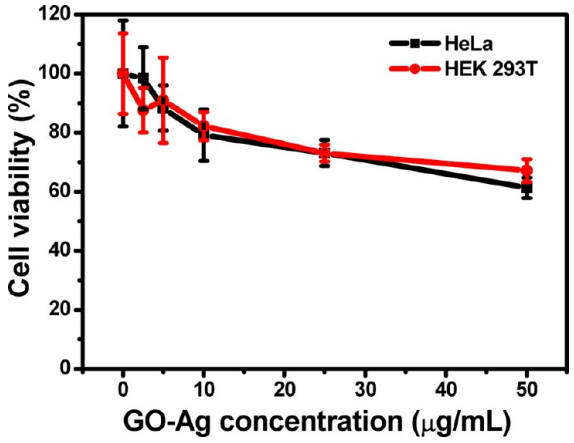

Figure 8. Relative viabilities of HeLa cells and HEK 293T cells after being exposed to GO−Ag nanocomposite (Ag:GO = 1:1) with different concentrations for 24 h. Error bars represent the standard deviations (n = 4).

4. CONCLUSION

In summary, an environmentally friendly, facile, simple, one-pot boiling method was developed to synthesize GO−Ag nanocomposites. With synergistically enhanced activity compared with AgNPs and the simple mixture of GO and AgNPs, our GO−Ag nanocomposite showed highly effective antibacterial activities at very low dosages, with an MIC of 4 μg/mL against *E. coli* and 14 μg/mL against *S. aureus*, possibly owing to the unique physicochemical properties of GO−Ag. Moreover, the different efficacies of GO−Ag nanocomposite against *E. coli* and *S. aureus* were uncovered, and all the data demonstrate that GO−Ag nanocomposite functions on these two types of bacteria through distinct, species-specific mechanisms: the high-performance of bactericidal effect of GO−Ag against the G− *E. coli* is due to bacterial cell wall/membrane integrity disruption, while the bacteriostatic effect against the G+ *S. aureus* is by inhibiting cell division. Future efforts, however, are still needed to further study the antibacterial mechanisms of GO−Ag at molecular and/or proteomic levels, as well as to understand why the GO−Ag nanocomposite would offer synergistic antibacterial effect instead of addictive effect in comparison to bare GO and AgNPs. Nevertheless, the results in this work could significantly improve our understanding regarding how GO-based nanocomposite interacts with microbes, and further promote the future use of GO−Ag as a new generation of powerful antibacterial agent with a wide range of potential industrial and clinical applications.

■ ASSOCIATED CONTENT

Ⓢ Supporting Information

Additional characterization data of GO−Ag nanocomposites, including size distributions of AgNPs formed on GO sheets, XRD, and EDS spectra; bacterial cell viabilities after treatments with higher concentrations GO−Ag nanocomposite (Ag:GO = 0.65:1) and pure AgNPs; agarose gel electrophoresis analysis of bacterial genomic DNA. This material is available free of charge via the Internet at http://pubs.acs.org.

■ AUTHOR INFORMATION

Corresponding Author

*E-mail: rpeng@suda.edu.cn (R.P.); zliu@suda.edu.cn (Z.L.).

Notes

The authors declare no competing financial interest.

■ ACKNOWLEDGMENTS

We thank Dr. Jie Xiao for useful comments and discussions. This work is supported by the National Basic Research Program of China (973 Program, 2012CB932600 and 2011CB911000), NSFC (51132006, 31070707, 91027039, 51002100), the Research Fund for the Doctoral Program of Higher Education of China (20103201120021), and a project funded by the Priority Academic Program Development of Jiangsu Higher Education Institutions (PAPD).

■ REFERENCES

(1) Levy, S. B.; Marshall, B. *Nat. Med.* **2004**, *10*, S122−S1229.
(2) Martinez, M.; Silley, P. *Handb. Exp. Pharmacol.* **2010**, *199*, 227−264.
(3) Payne, D. J.; Gwynn, M. N.; Holmes, D. J.; Pompliano, D. L. *Nat. Rev. Drug. Discov.* **2007**, *6*, 29−40.
(4) Wood, A. J. J.; Gold, H. S.; Moellering, R. C., Jr *N. Engl. J. Med.* **1996**, *335*, 1445−1453.
(5) Mauter, M. S.; Elimelech, M. *Environ. Sci. Technol.* **2008**, *42*, 5843−5859.
(6) Dastjerdi, R.; Montazer, M. *Colloids Surf., B* **2010**, *79*, 5−18.
(7) Seil, J. T.; Webster, T. J. *Int. J. Nanomedicine* **2012**, *7*, 2767−2781.
(8) Kim, J. S.; Kuk, E.; Yu, K. N.; Kim, J.-H.; Park, S. J.; Lee, H. J.; Kim, S. H.; Park, Y. K.; Park, Y. H.; Hwang, C.-Y.; Kim, Y.-K.; Lee, Y.-S.; Jeong, D. H.; Cho, M.-H. *Nanomed. Nanotechnol.* **2007**, *3*, 95−101.
(9) Marambio-Jones, C.; Hoek, E. M. V. *J. Nanopart. Res.* **2010**, *12*, 1531−1551.
(10) Martínez-Castañón, G. A.; Niño-Martínez, N.; Martínez-Gutierrez, F.; Martínez-Mendoza, J. R.; Ruiz, F. *J. Nanopart. Res.* **2008**, *10*, 1343−1348.
(11) Pal, S.; Tak, Y. K.; Song, J. M. *Appl. Environ. Microbiol.* **2007**, *73*, 1712−1720.
(12) Shrivastava, S.; Bera, T.; Roy, A.; Singh, G.; Ramachandrarao, P.; Dash, D. *Nanotechnology* **2007**, *18*, 225103.
(13) Ang, P. K.; Chen, W.; Wee, A. T. S.; Loh, K. P. *J. Am. Chem. Soc.* **2008**, *130*, 14392−14393.
(14) Feng, L.; Liu, Z. *Nanomedicine* **2011**, *6*, 317−324.
(15) He, S.; Song, B.; Li, D.; Zhu, C.; Qi, W.; Wen, Y.; Wang, L.; Song, S.; Fang, H.; Fan, C. *Adv. Funct. Mater.* **2010**, *20*, 453−459.
(16) Loh, K. P.; Bao, Q.; Eda, G.; Chhowalla, M. *Nat. Chem.* **2010**, *2*, 1015−1024.
(17) Shen, H.; Zhang, L.; Liu, M.; Zhang, Z. *Theranostics* **2012**, *2*, 283−294.
(18) Zhang, Y.; Nayak, T. R.; Hong, H.; Cai, W. *Nanoscale* **2012**, *4*, 3833−3842.
(19) Yang, K.; Zhang, S.; Zhang, G.; Sun, X.; Lee, S. T.; Liu, Z. *Nano Lett.* **2010**, *10*, 3318−3323.
(20) Yao, J.; Sun, Y.; Yang, M.; Duan, Y. *J. Mater. Chem.* **2012**, *22*, 14313.
(21) Zuo, X.; He, S.; Li, D.; Peng, C.; Huang, Q.; Song, S.; Fan, C. *Langmuir* **2009**, *26*, 1936−1939.
(22) Feng, L.; Wu, L.; Qu, X. *Adv. Mater.* **2013**, *25*, 168−186.
(23) Zhao, F.; Zhao, Y.; Liu, Y.; Chang, X.; Chen, C.; Zhao, Y. *Small* **2011**, *7*, 1322−1337.
(24) Tan, X.; Feng, L.; Zhang, J.; Yang, K.; Zhang, S.; Liu, Z.; Peng, R. *ACS Appl. Mater. Interfaces* **2013**, *5*, 1370−1377.
(25) Qu, K.; Wu, L.; Ren, J.; Qu, X. *ACS Appl. Mater. Interfaces* **2012**, *4*, 5001−5009.
(26) Song, Y.; Qu, K.; Zhao, C.; Ren, J.; Qu, X. *Adv. Mater.* **2010**, *22*, 2206−2210.
(27) Bao, H.; Pan, Y.; Ping, Y.; Sahoo, N. G.; Wu, T.; Li, L.; Li, J.; Gan, L. H. *Small* **2011**, *7*, 1569−1578.
(28) Depan, D.; Shah, J.; Misra, R. D. K. *Mater. Sci. Eng., C* **2011**, *31*, 1305−1312.
(29) Kakran, M.; Sahoo, N. G.; Bao, H.; Pan, Y.; Li, L. *Curr. Med. Chem.* **2011**, *18*, 4503−4512.
(30) Ma, D.; Lin, J.; Chen, Y.; Xue, W.; Zhang, L.-M. *Carbon* **2012**, *50*, 3001−3007.
(31) Sahoo, N. G.; Bao, H.; Pan, Y.; Pal, M.; Kakran, M.; Cheng, H. K. F.; Li, L.; Tan, L. P. *Chem. Commun.* **2011**, *47*, 5235−5237.
(32) Yang, X.; Wang, Y.; Huang, X.; Ma, Y.; Huang, Y.; Yang, R.; Duan, H.; Chen, Y. *J. Mater. Chem.* **2011**, *21*, 3448−3454.
(33) Zhang, L.; Lu, Z.; Zhao, Q.; Huang, J.; Shen, H.; Zhang, Z. *Small* **2011**, *7*, 460−464.
(34) Zhang, L. M.; Xia, J. G.; Zhao, Q. H.; Liu, L. W.; Zhang, Z. J. *Small* **2010**, *6*, 537−544.
(35) Liu, Z.; Robinson, J. T.; Sun, X.; Dai, H. *J. Am. Chem. Soc.* **2008**, *130*, 10876−10877.
(36) Chen, B.; Liu, M.; Zhang, L.; Huang, J.; Yao, J.; Zhang, Z. *J. Mater. Chem.* **2011**, *21*, 7736−7741.
(37) Feng, L.; Zhang, S.; Liu, Z. *Nanoscale* **2011**, *3*, 1252−1257.
(38) Kim, H.; Namgung, R.; Singha, K.; Oh, I.-K.; Kim, W. J. *Bioconjugate Chem* **2011**, *22*, 2558−2567.
(39) He, Q.; Sudibya, H. G.; Yin, Z.; Wu, S.; Li, H.; Boey, F.; Huang, W.; Chen, P.; Zhang, H. *ACS Nano* **2010**, *4*, 3201−3208.
(40) Tang, L. A. L.; Wang, J.; Loh, K. P. *J. Am. Chem. Soc.* **2010**, *132*, 10976−10977.
(41) Liu, Y.; Dong, X.; Chen, P. *Chem. Soc. Rev.* **2012**, *41*, 2283−307.
(42) Song, Y.; Wei, W.; Qu, X. *Adv. Mater.* **2011**, *23*, 4215−4236.
(43) Zhang, X.; Yin, J.; Peng, C.; Hu, W.; Zhu, Z.; Li, W.; Fan, C.; Huang, Q. *Carbon* **2011**, *49*, 986−995.
(44) Yang, K.; Feng, L.; Shi, X.; Liu, Z. *Chem. Soc. Rev.* **2013**, *42*, 530−547.
(45) Yang, K.; Hu, L.; Ma, X.; Ye, S.; Cheng, L.; Shi, X.; Li, C.; Li, Y.; Liu, Z. *Adv. Mater.* **2012**, *24*, 1868−1872.
(46) Yang, K.; Wan, J.; Zhang, S.; Zhang, Y.; Lee, S.-T.; Liu, Z. *ACS Nano* **2010**, *5*, 516−522.
(47) Akhavan, O.; Ghaderi, E. *ACS Nano* **2010**, *4*, 5731−5736.
(48) Hu, W.; Peng, C.; Luo, W.; Lv, M.; Li, X.; Li, D.; Huang, Q.; Fan, C. *ACS Nano* **2010**, *4*, 4317−4323.
(49) Liu, S.; Zeng, T. H.; Hofmann, M.; Burcombe, E.; Wei, J.; Jiang, R.; Kong, J.; Chen, Y. *ACS Nano* **2011**, *5*, 6971−6980.
(50) Ruiz, O. N.; Fernando, K. A. S.; Wang, B.; Brown, N. A.; Luo, P. G.; McNamara, N. D.; Vangsness, M.; Sun, Y.-P.; Bunker, C. E. *ACS Nano* **2011**, *5*, 8100−8107.
(51) Yang, K.; Li, Y.; Tan, X.; Peng, R.; Liu, Z. *Small* **2012**, DOI: 10.1002/smll.201201417.
(52) Yin, S.; Goldovsky, Y.; Herzberg, M.; Liu, L.; Sun, H.; Zhang, Y.; Meng, F.; Cao, X.; Sun, D. D.; Chen, H.; Kushmaro, A.; Chen, X. *Adv. Funct. Mater.* **2013**, DOI: 10.1002/adfm.201203491.
(53) Bao, Q.; Zhang, D.; Qi, P. *J. Colloid Interface Sci.* **2011**, *360*, 463−470.
(54) Chook, S.; Chia, C.; Zakaria, S.; Ayob, M.; Chee, K.; Huang, N.; Neoh, H.; Lim, H.; Jamal, R.; Rahman, R. *Nanoscale Res. Lett.* **2012**, *7*, 1−7.
(55) Das, M. R.; Sarma, R. K.; Saikia, R.; Kale, V. S.; Shelke, M. V.; Sengupta, P. *Colloids Surf., B* **2011**, *83*, 16−22.
(56) Liu, L.; Liu, J.; Wang, Y.; Yan, X.; Sun, D. D. *New J. Chem.* **2011**, *35*, 1418.
(57) Ma, J.; Zhang, J.; Xiong, Z.; Yong, Y.; Zhao, X. S. *J. Mater. Chem.* **2011**, *21*, 3350.
(58) Pasricha, R.; Gupta, S.; Srivastava, A. K. *Small* **2009**, *5*, 2253−2259.
(59) Shen, J.; Shi, M.; Li, N.; Yan, B.; Ma, H.; Hu, Y.; Ye, M. *Nano Res.* **2010**, *3*, 339−349.
(60) Shen, J.; Shi, M.; Yan, B.; Ma, H.; Li, N.; Ye, M. *J. Mater. Chem.* **2011**, *21*, 7795−7801.
(61) Tang, X. Z.; Cao, Z.; Zhang, H. B.; Liu, J.; Yu, Z. Z. *Chem. Commun.* **2011**, *47*, 3084−3086.
(62) Wang, X.; Huang, P.; Feng, L.; He, M.; Guo, S.; Shen, G.; Cui, D. *RSC Adv.* **2012**, *2*, 3816.
(63) Xu, W.-P.; Zhang, L.-C.; Li, J.-P.; Lu, Y.; Li, H.-H.; Ma, Y.-N.; Wang, W.-D.; Yu, S.-H. *J. Mater. Chem.* **2011**, *21*, 4593.

(64) Zhang, Z.; Xu, F.; Yang, W.; Guo, M.; Wang, X.; Zhang, B.; Tang, J. *Chem. Commun.* **2011**, *47*, 6440−2.
(65) Osborn, M. J. *Annu. Rev. Biochem.* **1969**, *38*, 501−538.
(66) Sun, X.; Liu, Z.; Welsher, K.; Robinson, J. T.; Goodwin, A.; Zaric, S.; Dai, H. *Nano Res.* **2008**, *1*, 203−212.
(67) Jin, L.; Yang, K.; Yao, K.; Zhang, S.; Tao, H.; Lee, S.-T.; Liu, Z.; Peng, R. *ACS Nano* **2012**, *6*, 4864−4875.
(68) Dagnall, R. M.; West, T. S. *Talanta* **1961**, *8*, 711−719.
(69) Ciapetti, G.; Cenni, E.; Pratelli, L.; Pizzoferrato, A. *Biomaterials* **1993**, *14*, 359−364.
(70) Wiegand, I.; Hilpert, K.; Hancock, R. E. *Nat. Protoc.* **2008**, *3*, 163−175.
(71) Xie, X. S.; Choi, P. J.; Li, G.-W.; Lee, N. K.; Lia, G. *Annu. Rev. Biophys. Biomol. Struct.* **2008**, *37*, 417−444.
(72) Simon, M. C.; Gray, D. I.; Cook, N. *Appl. Environ. Microbiol.* **1996**, *62*, 822−4.
(73) Yang, J.; Balasundaram, G.; Lo, S.-L.; Guang, E. C. S.; Xue, J. M.; Song, J.; Wan, A. C. A.; Ying, J. Y.; Wang, S. *Adv. Mater.* **2012**, *24*, 3280−3284.
(74) Jung, W. K.; Koo, H. C.; Kim, K. W.; Shin, S.; Kim, S. H.; Park, Y. H. *Appl. Environ. Microbiol.* **2008**, *74*, 2171−2178.